Energy density engineering via zero-admittance domains in all-dielectric stratified materials

Claude Amra,[1,*] Myriam Zerrad,[1] Fabien Lemarchand,[1] Aude Lereu,[1] Ali Passian,[2]
Juan Antonio Zapien,[3] and Michel Lequime[1]

[1]*Aix Marseille Univ, CNRS, Centrale Marseille, Institut Fresnel, Faculté des Sciences–Campus Saint Jérôme,
Avenue Escadrille Normandie-Niémen, 13397 Marseille, France*
[2]*Quantum Information Science, Oak Ridge National Laboratory, 1 Bethel Valley Road, Oak Ridge, Tennessee 37830, USA*
[3]*Center Of Super-Diamond and Advanced Films (COSDAF) and Department of Materials Science and Engineering,
City University of Hong Kong, Hong Kong, SAR, People's Republic of China*

Emerging photonic, sensing, and quantum applications require high fields and tight localization but low power consumption. Spatial, spectral, and magnitude control of electromagnetic fields is of key importance for enabling experiments in atomic, molecular, and optical physics. We introduce the concept of zero-admittance domains as a mechanism for tailoring giant optical fields bound within or on the surface of dielectric media. The described mechanism permits the creation of highly localized fields of extreme amplitudes simultaneously for incident photons of multiple wavelengths and incidence angles but arbitrary polarization states. No material constraints are placed upon the bounding media. Both intrinsic and extrinsic potential practical limitations of the predicted field enhancement are analyzed and applications relevant to optical sensors and microsources are briefly discussed.

I. INTRODUCTION

Stratified media are a well-investigated material class in physics. Nevertheless, due to the high degrees of freedom with respect to the material types of each domain, the domain's geometric configurations, and excitation channels, novel electromagnetic effects continue to be discovered [1–14]. Importantly, field enhancement and volume confinement of electromagnetic energy continue to promote key applications such as those related to miniaturized sensors, super-resolution microscopy, tip- and surface-enhanced spectroscopy, microsources, and excitation and readout of quantum emitters. A variety of approaches, such as photonic crystals and metamaterials, optical multilayers, overlayered gratings, microrings, and microspheres [15–23], have been explored to achieve control over the field properties. While within this framework, metal-based approaches using plasmonic structures have been extensively studied [22–27], more recently, systems based on dielectric media are being increasingly explored [28–35]. In particular, all-dielectric multilayers are emerging as a highly versatile approach to field enhancement engineering [28–32]. For frequencies within the optical regime, a metallic medium, e.g., a thin film of gold, exhibits finite losses measured by the magnitude of the imaginary part of its dielectric function, leading to plasmon dissipation rate measured by the imaginary part of the plasmon wave vector. Unlike metallic systems [7,9], where collective electronic effects provide useful resonance spectra, albeit often with significant dissipation, solid-state lossless or low-loss dielectric thin-film multilayers provide ultrasharp resonances with little or negligible dissipation.

Control of specular properties such as energy coefficients (reflection, transmission), phase and polarization, coherence, and pulse shaping is often achieved in free space by capitalizing on interference effects in periodic stratified media (e.g., optical interference coatings [36,37]). Such media are often referred to as one-dimensional (1D) photonic crystals, and their related field properties and enhancements are being associated with Bloch surface modes [38,39]. Thin-film designers, through developing modern design techniques [40,41], can now produce multidielectric devices with nearly 1000 thin-film layers, so as to satisfy a growing number of constraints. These interferential filters have not been commonly considered for field enhancement. In fact, narrow-band filters in free space may exhibit such properties, though the achieved enhancement is confined within their spacer layers, yielding no sensitivity to the surrounding medium. For this reason, several works [28–35] were devoted to the study of resonance spectra of all-dielectric multilayer media under the condition of total internal reflection (TIR), so as to create a high-intensity field bound to the free interface. However, due to lack of an optimization concept and its analytic formulation, a design method has not been fully achieved until now. As a result, most often numerical data have been used to identify the reflection poles of the structure, without any additional control, extension, or generalization.

In this work, we introduce the concept of zero-admittance layers (ZALs) to control and optimize the electromagnetic response of the material. The ZALs are proposed to be made of standard dielectric materials with optical thicknesses that can be adjusted with respect to submultilayers. Subsequently, we show that several ZALs can be introduced to achieve an optimized system that exhibits multiwavelength or multiangle field enhancement. The proposed approach is presented as follows. We begin by showing how the new layers allow

*claude.amra@fresnel.fr

a reversal of the depth field distribution within a periodic stratified dielectric material (stack), and provide giant optimization. Then we extend the procedure for arbitrary substrates and depth localization within the multilayer. Eventually, we generalize the concept and describe how to obtain resonances at specific sets of illumination angles and wavelengths. In the last sections, in order to enable future experimental investigation, we analyze the predicted field enhancement to assess which realistic parameter ranges can be reached. We end our presentation by discussing intrinsic and extrinsic limitations pertaining to absorption and illumination bandpasses (spectral width and divergence), as well as to the design accuracy.

II. MATRIX FORMALISM IN OPTICAL MULTILAYERS

Thin-film multilayers constitute a central material system in the proposed concept. We therefore begin by considering an all-dielectric system deposited on a transparent substrate with a real refractive index n_s (Fig. 1). Within a harmonic (monochromatic) regime, the spatial pulsation σ is given by the illumination conditions, that is,

$$\sigma = \frac{2\pi}{\lambda} n_0 \sin\theta_0 = k_0 \sin\theta_0 < k_0, \qquad (1)$$

where λ is the wavelength of the incident field in vacuum; θ_0 is the illumination angle in the incident medium, that is, the superstrate with a real refractive index n_0. We note that there is one cutoff frequency $k_s = 2\pi n_s/\lambda$, which defines the range

of the TIR, that is (see Fig. 1),

$$\sigma > k_s = \frac{2\pi}{\lambda} n_s \Rightarrow T = 0 \text{ and } R = 1 - A, \qquad (2)$$

with R, T being the reflection and transmission energy coefficients, and A the absorption. In what follows, we neglect the slight absorption of the dielectric thin films ($A \approx 0$), since their imaginary indices are often lower than 10^{-5} [24,25].

Assuming that all materials are linear, isotropic, homogeneous, and nonmagnetic, the matrix formalism [22] allows one to connect the tangential electric and magnetic fields at interfaces $(i - 1)$ and (i) as follows:

$$\begin{pmatrix} E_{i-1} \\ H_{i-1} \end{pmatrix} = M_i \begin{pmatrix} E_i \\ H_i \end{pmatrix}, \ M_i = \begin{pmatrix} \cos\delta_i & -\left(\frac{j}{\tilde{n}_i}\right)\sin\delta_i \\ -j\tilde{n}_i\sin\delta_i & \cos\delta_i \end{pmatrix}, \tag{3}$$

where M_i denotes the matrix of layer (i) written for a temporal field variation in the form $\exp(-j\omega t)$, and δ_i is a dimensionless phase term and $\tilde{n}_i$ is the polarization-dependent effective index, given by

$$\tilde{n}_i = \begin{cases} n_i\alpha_i/k_i & \text{for TE or s polarization of light} \\ n_i k_i/\alpha_i & \text{for TM or p polarization of light} \end{cases}, \tag{4}$$

$$\delta_i = \alpha_i e_i, \tag{5}$$

$$\alpha_i = \sqrt{k_i^2 - \sigma^2}, \quad k_i = 2\pi n_i/\lambda, \quad \sigma = k_i \sin\theta_i, \tag{6}$$

with e_i and n_i being the thickness and refractive index of layer i. Following the Snell-Descartes law, the spatial pulsation σ is invariant with the medium. Though all materials are assumed transparent, introduction of real propagation angles is not always possible in all media, as was done in Eq. (6). Actually, this would require the condition $\sigma < k_i$, which is not guaranteed for all layers except for when the superstrate is vacuum ($\sigma < k_0 < k_i$). Therefore, it is preferable to work with spatial pulsations rather than angles.

As usual, quarter-wave stacks (QWSs) are most often used in thin-film techniques due to their stationary properties. Here, they greatly simplify the layer matrix (3) as

$$\delta_i = \frac{\pi}{2} \Rightarrow M_i = -j\begin{pmatrix} 0 & 1/\tilde{n}_i \\ \tilde{n}_i & 0 \end{pmatrix}, \tag{7}$$

which is valid for matched layers, that is, layers with optical thicknesses that are quarter wave at incidence θ_i and wavelength λ_0, specifically:

$$\delta_i = \alpha_i e_i = \frac{\pi}{2} \Rightarrow n_i e_i \cos\theta_i = \lambda_0/4. \tag{8}$$

Such condition requires α_i to be real, and hence the stationary field distribution is trigonometric within layer i under the following condition:

$$\text{Im}(\alpha_i) = 0 \Leftrightarrow \sigma < k_i. \tag{9}$$
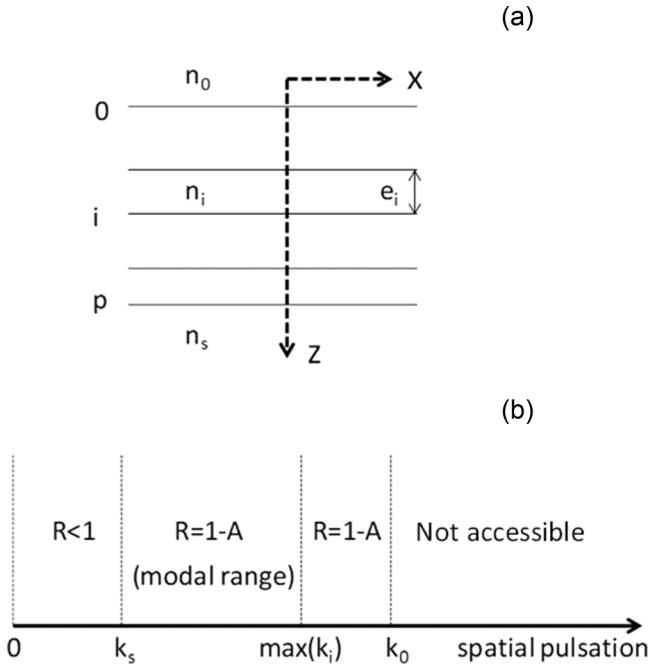
FIG. 1. Schematic presentation of an all-dielectric planar multilayer thin-film system. Geometry of design (a) and various reflection regimes as a function of the in-plane wave vector σ (b) for a free space illumination ($\sigma < k_0$). Light, propagating in the z direction, enters layer i with a thickness e_i and a refractive index of n_i. Below k_s, TIR is compromised.

We now consider a series of four quarter-wave Q_m structures given by

$$
\begin{aligned}
Q_1 &= (LH)^N S, \\
Q_2 &= (HL)^N S, \\
Q_3 &= H(LH)^N S, \\
Q_4 &= L(HL)^N S,
\end{aligned}
$$

where notations H and L are used for high- and low-index quarter-wave layers, respectively, the letter S is for the substrate, while the incident medium (superstrate) is not specified. The number of layers is $p = 2N$ for $Q_{m=1,2}$ or $p = 2N + 1$ for $Q_{m=3,4}$. The Q_m structures are classical quarter-wave mirrors matched for the illumination conditions (λ_0, θ_0).

We assume that the illumination conditions satisfy relation (9), that is,

$$
0 < \sigma < k_L < k_H, \tag{10}
$$

so that all matrix coefficients are real. From (7), it is straightforward to check that

$$
M_{i-1} M_i = -\begin{pmatrix} \tilde{n}_i / \tilde{n}_{i-1} & 0 \\ 0 & \tilde{n}_{i-1} / \tilde{n}_i \end{pmatrix}, \tag{11}
$$

that is, for a couple of layers,

$$
M_L M_H = M_{LH} = -\begin{pmatrix} \beta & 0 \\ 0 & 1/\beta \end{pmatrix}, \tag{12}
$$

$$
M_H M_L = M_{HL} = -\begin{pmatrix} 1/\beta & 0 \\ 0 & \beta \end{pmatrix}, \tag{13}
$$

where β denotes the ratio of the effective indices:

$$
\beta = \tilde{n}_H / \tilde{n}_L. \tag{14}
$$

Hence the stack matrices Q_m follow for each structure:

$$
\begin{aligned}
Q_1 &= (-1)^N \begin{pmatrix} \beta^N & 0 \\ 0 & \frac{1}{\beta^N} \end{pmatrix}, \\
Q_2 &= (-1)^N \begin{pmatrix} 1/\beta^N & 0 \\ 0 & \beta^N \end{pmatrix}, \\
Q_3 &= -j\,(-1)^N \begin{pmatrix} 0 & 1/(\tilde{n}_H \beta^N) \\ \tilde{n}_H \beta^N & 0 \end{pmatrix}, \\
Q_4 &= -j\,(-1)^N \begin{pmatrix} 0 & \beta^N / \tilde{n}_L \\ \tilde{n}_L / \beta^N & 0 \end{pmatrix}.
\end{aligned} \tag{15}
$$

III. LIMITATION OF THE CLASSICAL FIELD ENHANCEMENT

In order to quantitatively calculate the field enhancement, we proceed by introducing the complex admittance Y [22]:

$$
\left(\frac{E_s}{E_0} \right)_m = \frac{1}{a_m + b_m Y_s} = \frac{Y_{0,m}}{c_m + d_m Y_s}, \tag{16}
$$

with

$$
Y_{0,m} = \frac{c_m + d_m Y_s}{a_m + b_m Y_s}, \tag{17}
$$

where E_0 and E_s designate the total tangential electric fields at the top (0) and bottom (s) surfaces, while $Y_{0,m}$ and Y_s are the corresponding stack admittances. The other coefficients are given by the stack matrix written as

$$
Q_m = \begin{pmatrix} a_m & b_m \\ c_m & d_m \end{pmatrix}. \tag{18}
$$

The admittance is given by the ratio of the tangential magnetic and electric fields,

$$
\vec{H} = Y(\vec{z} \wedge \vec{E}), \tag{19}
$$

where $\vec{z}$ is the stack normal (Fig. 1). This Y quantity is polarization and z dependent, and reduces to the effective index $\pm \tilde{n}$ in the case of nonstationary (retrograde or progressive) waves, which happens in the substrate:

$$
Y_s = \tilde{n}_s. \tag{20}
$$

We can now develop the expressions for field enhancement depending upon the chosen stack Q_m. Following (16), the enhancement is first given for each proposed structure as

$$
\left| \frac{E_s}{E_0} \right|^2 =
\begin{cases}
\frac{1}{\beta^{2N}} & \text{for } Q_1 = (LH)^N S \\[4pt]
\beta^{2N} & \text{for } Q_2 = (HL)^N S \\[4pt]
\beta^{2N} \left| \frac{\tilde{n}_H}{Y_s} \right|^2 & \text{for } Q_3 = H(LH)^N S \\[4pt]
\frac{1}{\beta^{2N}} \left| \frac{\tilde{n}_L}{Y_s} \right|^2 & \text{for } Q_4 = L(HL)^N S
\end{cases}, \tag{21}
$$

which is valid in the low-spatial-pulsation regime ($\sigma < k_L < k_H$). Thus the field is trigonometric in all media (real α_H and α_L values), allowing all layers to be matched in a quarter-wave form. The ratio $|E_s / E_0|^2$ can be increased or decreased, depending on the stack and on whether $\beta < 1$ or $\beta > 1$. However, the enhancement must be calculated with respect to the incident field E_0^+ (as opposed to the stationary field E_0). The progressive field E_0^+ is proportional to the total field E_0 at the top surface depending upon the amplitude reflection factor r, that is,

$$
E_0 = (1 + r) E_0^+, \tag{22}
$$

with

$$
r = \frac{\tilde{n}_0 - Y_0}{\tilde{n}_0 + Y_0}. \tag{23}
$$

Consequently, the enhancement must be corrected as

$$
\left| \frac{E_s}{E_0^+} \right|^2 = |1 + r|^2 \left| \frac{E_s}{E_0} \right|^2 = \left| \frac{2\tilde{n}_0}{\tilde{n}_0 + Y_0} \right|^2 \left| \frac{E_s}{E_0} \right|^2. \tag{24}
$$

Following (17) and (18), the top surface admittances can be calculated for each structure as

$$
Y_0 =
\begin{cases}
\frac{Y_s}{\beta^{2N}} & \text{for } Q_1 = (LH)^N S \\[4pt]
Y_s \beta^{2N} & \text{for } Q_2 = (HL)^N S \\[4pt]
\tilde{n}_H^2 \frac{\beta^{2N}}{Y_s} & \text{for } Q_3 = H(LH)^N S \\[4pt]
\frac{1}{\beta^{2N}} \frac{\tilde{n}_H^2}{Y_s} & \text{for } Q_4 = L(HL)^N S
\end{cases}, \tag{25}
$$
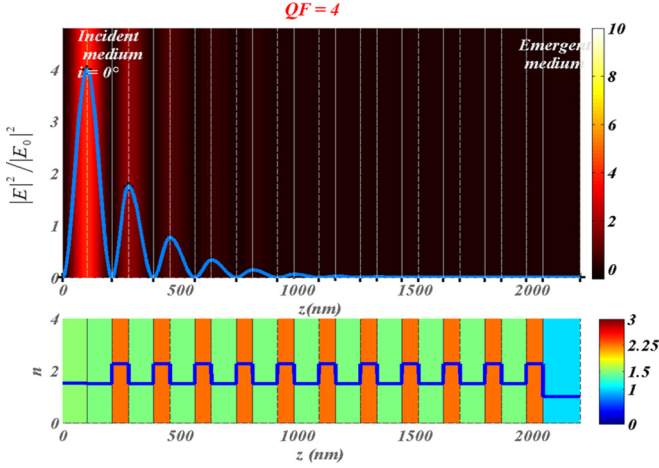
FIG. 2. Classical field distribution within a quarter-wave mirror at normal illumination (top), and the corresponding design indices (bottom) versus thickness. The incident wavelength is the design wavelength ($\lambda = \lambda_0 = 633$ nm). Materials are Ta_2O_5/SiO_2. The normalized field is maximum in the incident medium with a value close to 4.

which when used in conjunction with (21)–(25) yields the final result:

$$\left| \frac{E_s}{E_0^+} \right|^2 = \begin{cases} \beta^{2N} \left| \frac{2\tilde{n}_0}{Y_s + \tilde{n}_0 \beta^{2N}} \right|^2 & \text{for } Q_1 = (LH)^N S \\ \beta^{2N} \left| \frac{2\tilde{n}_0}{\tilde{n}_0 + Y_s \beta^{2N}} \right|^2 & \text{for } Q_2 = (HL)^N S \\ \tilde{n}_H^2 \beta^{2N} \left| \frac{2\tilde{n}_0}{\tilde{n}_0 Y_s + \tilde{n}_H^2 \beta^{2N}} \right|^2 & \text{for } Q_3 = H(LH)^N S \\ \tilde{n}_L^2 \beta^{2N} \left| \frac{2\tilde{n}_0}{\tilde{n}_H^2 + \tilde{n}_0 Y_s \beta^{2N}} \right|^2 & \text{for } Q_4 = L(HL)^N S \end{cases} \tag{26}$$

Thus all enhancement vanishes when the number of layers increases, so that the field is always maximum in the vicinity of the top surface and strongly decreases as it approaches the substrate (see Fig. 2), explicitly,

$$\lim_{N \to \infty} |E_s/E_0^+|^2 = 0. \tag{27}$$

The above result is valid regardless of the β values ($\beta < 1$ or $\beta > 1$), which is classical and characteristic of a quarter-wave mirror. Also, it is valid regardless of the reflection regime, that is, TIR or otherwise, since we did not assume $\sigma < k_s$ or $\sigma > k_s$, but only forced the field to be trigonometric in all layers ($\sigma < k_L < k_H$) so as to satisfy the matching condition. Hence we conclude that no enhancement can occur at the substrate surface with these Q_m structures (see Fig. 2).

IV. ACHIEVING ENHANCEMENT VIA THE CONCEPT OF TIR ZERO-ADMITTANCE LAYER

To circumvent the above impasse, we note that in relations (26), there is one degree of freedom, related to the substrate admittance ($Y_s = \tilde{n}_s \neq 0$), which was not explored. According to relations (4), the substrate effective index $\tilde{n}_s$ is a given quantity and cannot be zero regardless of polarization, incidence angle, and wavelength of the incoming photons. However, we will now show how a zero-starting admittance

can be achieved under TIR to allow the reversal of the field depth dependence while providing a strong enhancement at the substrate surface. The admittance cancellation can be shown to modify the asymptotic behavior of the enhancement versus the β parameter. Noting that the admittance obeys the recurrence,

$$Y_{i-1} = \frac{-j\tilde{n}_i \sin\delta_i + Y_i \cos\delta_i}{\cos\delta_i - jY_i \sin\delta_i/\tilde{n}_i}, \tag{28}$$

we aim at canceling the substrate admittance $\tilde{n}_s$ with the deposition of a single layer of phase δ_p and refractive index n_p, to obtain:

$$Y_s = \tilde{n}_s \Rightarrow Y_{p-1} = \frac{-j\tilde{n}_p \sin\delta_p + \tilde{n}_s \cos\delta_p}{\cos\delta_p - \frac{j\tilde{n}_s \sin\delta_p}{\tilde{n}_p}} = 0$$
$$\Rightarrow \tan\delta_p = -j\tilde{n}_s/\tilde{n}_p. \tag{29}$$

Let us first search for solutions below the frequency limit of TIR ($\sigma < k_s$), where the effective index $\tilde{n}_s$ is real. Furthermore, we used trigonometric fields ($\sigma < k_L < k_H$) so that all effective indices $\tilde{n}_i$ are also real (quarter wave with real δ_i). Therefore, relation (29) cannot be satisfied ($\tilde{n}_s/\tilde{n}_p$ is real while $\tan\delta_p$ is purely imaginary). Introduction of a third thin-film material would not modify this result.

Hence deposition of a single layer between the QWS and the substrate does not facilitate the cancellation of the starting admittance. More generally, we establish that multilayers do not either allow such cancellation of the admittance except for in the asymptotic limit when the number of layers goes to infinity. Also, we note that since the enhancement ratio at the bottom surface is connected with the amplitude transmission factor $t = E_s^+/E_0^+$, it is bounded by $\tilde{n}_0/\tilde{n}_s$, in accordance with the energy balance:

$$T = \left(\frac{\tilde{n}_s}{\tilde{n}_0} \right) |t|^2 < 1 \Rightarrow |t|^2 = |E_s^+/E_0^+|^2 < \tilde{n}_0/\tilde{n}_s. \tag{30}$$

Therefore, we explore the higher spatial frequencies, that is, beyond the TIR regime ($\sigma > k_s$), where the substrate admittance $\tilde{n}_s$ is purely imaginary and there is no energy transport in the substrate, where the field is evanescent since the Poynting flux is proportional to [42]

$$\phi_s^+ = \text{Re}(\tilde{n}_s)|E_s^+|^2 = 0. \tag{31}$$

Consequently, the amplitude transmission factor t (and so the enhancement) is no longer bounded at TIR since it is not involved in the energy balance, now given by $1 = R + A$. Thus

$$T = \frac{\text{Re}(\tilde{n}_s)}{\tilde{n}_0} |t|^2 = 0, \tag{32}$$

regardless of the amplitude t. Owing to these remarks, TIR offers the opportunity to build a ZAL. Indeed since $\tilde{n}_s$ is purely imaginary, the $\tan\delta_p$ term of (29) is now real, yielding

$$\tan\delta_p = \text{Im}(\tilde{n}_s)/\tilde{n}_p, \tag{33}$$

which allows the design of a thin film (thickness e_p, effective index $\tilde{n}_p$ with $\sigma < k_p$,) that makes the admittance vanish at the surface ($p - 1$). Such substrate over-coating will now reverse the field distribution within the stack and provide a huge enhancement. Indeed, within this TIR range, $k_s < \sigma < k_L < k_H$, we assemble the preceding quarter-wave structures
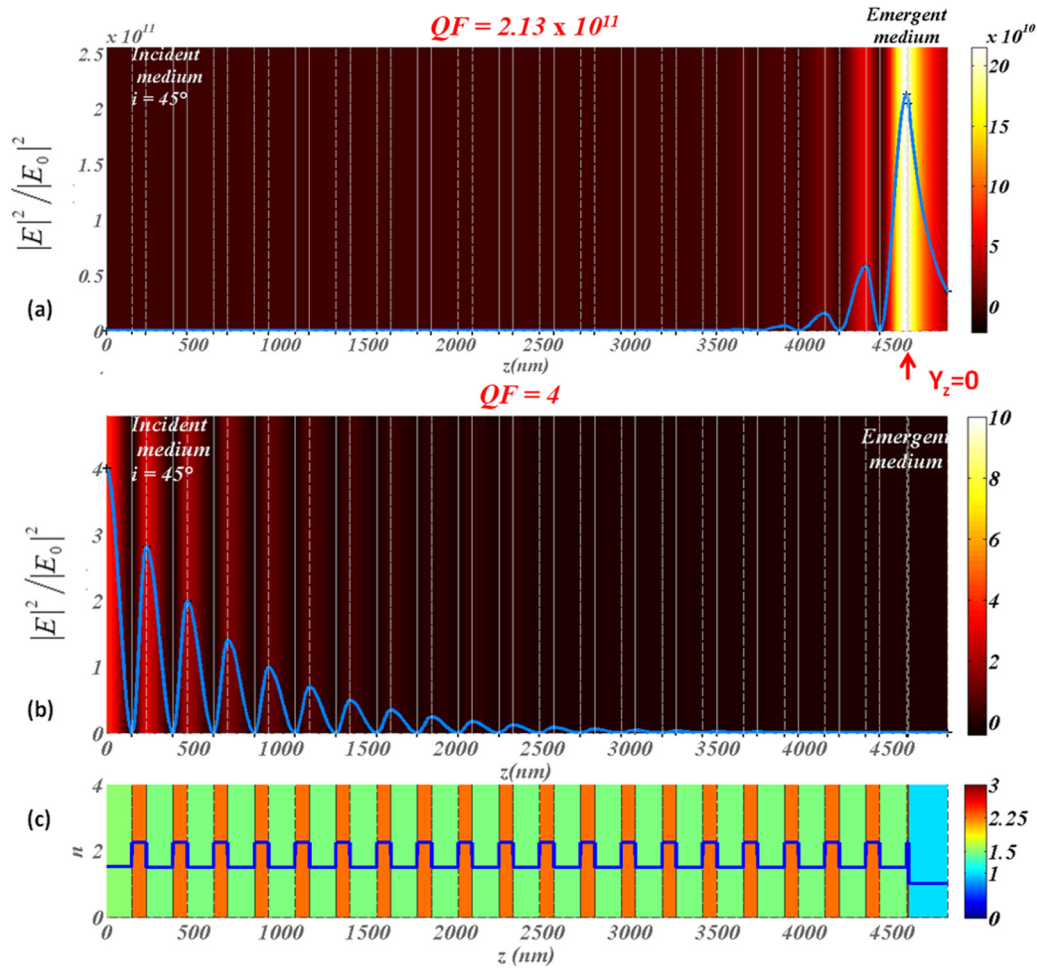
FIG. 3. The proposed concept of zero-admittance layer (ZAL) generating huge field enhancement. The ZAL (designed with $n_p = n_H$) is inserted between the QWS and the substrate. The design is optimized for TE polarization (a) in the TIR range with $\theta = 45°$. The field is evanescent in the substrate (on the right). The incident wavelength is the design wavelength ($\lambda = \lambda_0 = 633$ nm). Materials are Ta$_2$O$_5$/SiO$_2$. TM polarization is plotted for comparison in (b). The ZAL is localized near the substrate as indicated by the arrow $Y_z = 0$. The employed design profile as a function of index and thickness is shown in (c).

Q_m on the zero-admittance precoated substrate. Introducing $Y_s = 0$ in (26) yields an enhancement:

$$\left| \frac{E_s}{E_0^+} \right|^2 = \begin{cases} 4/\beta^{2N} & \text{for } Q_1 = (LH)^N S \\ 4\beta^{2N} & \text{for } Q_2 = (HL)^N S \\ \frac{4}{\beta^{2N}} \left(\frac{\tilde{n}_0}{\tilde{n}_H} \right)^2 & \text{for } Q_3 = H(LH)^N S \\ 4\beta^{2N} \left(\frac{\tilde{n}_0}{\tilde{n}_L} \right)^2 & \text{for } Q_4 = L(HL)^N S \end{cases} \quad (34)$$

We have thus shown that it is feasible for the enhancement to occur close to the substrate surface, so that the field distribution may be considered reversed and the enhancement strongly amplified (see Fig. 3) when compared to those of Fig. 2. In Fig. 3, a Q_2-type structure was assumed for TE polarization [Fig. 3(a)] and 45° illumination incidence. Denoting the enhancement with QF, Fig. 3 shows a value of $QF = 2.13 \times 10^{11}$, which is in agreement with Eq. (34). Such value is not realistic and will be bounded by nonlinearities and damage thresholds [43,44] in materials, as well as by illumination band passes [28] and design accuracy. The case of TM polarization, given in Fig. 3(b), exhibits no enhancement. Remarkably, these highly

versatile properties are here achieved with a ZAL of only 10.03 nm thickness (not visible in Fig. 3).

In the proposed approach, depending on the Q_m structure, one needs to consider $\beta < 1$ (Q_1 and Q_3) or $\beta > 1$ (Q_2 and Q_4) to achieve the enhancement. Since the β parameter is polarization and angle dependent, one has to consider the functional form of $\beta(\sigma)$, as shown in Fig. 4. The plot in Fig. 4 emphasizes two properties in the frequency range of interest $[k_s, k_L]$:

(1) for TE polarization, $\beta > 1$ in the entire range so that Q_2 and Q_4 structures must be used to provide an enhancement,

(2) TM polarization exhibits a cutoff frequency at each side of which β is greater or lower than 1. This frequency corresponds to the Brewster effect at an H/L or L/H interface and is given by

$$\sigma_c = k_H k_L / \sqrt{k_H^2 + k_L^2}. \quad (35)$$

Therefore, at low frequencies $\sigma < \sigma_c$, $\beta > 1$ and TM polarization must be used with structures Q_2 and Q_4. Conversely, at higher frequencies $\sigma > \sigma_c$, $\beta < 1$ and TM polarization must be used with structures Q_1 and Q_3.
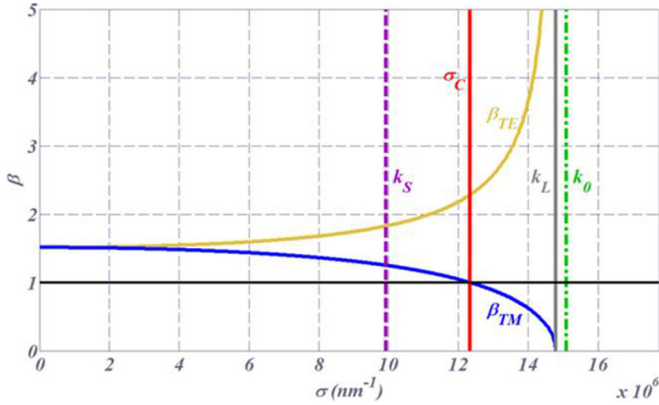
FIG. 4. The variation of the effective index ratio as a function of the spatial pulsation for TE and TM polarizations.

As a result, the structures suitable for both S and P polarizations are Q_2 and Q_4, provided that the frequencies lie in the range $k_L < \sigma < \sigma_c$. However, the efficiency will be much better when σ approaches k_L, hence leading to extreme β values (0 or ∞) with a faster enhancement with the number of layers. To give an order of magnitude, working with TE polarization at $\theta_0 = 70°$, provides an enhancement close to 10^4 with a stack of only six layers. For that reason, practical solutions will involve Q_2 and Q_4 for TE polarization, and Q_1 and Q_3 for TM polarization.

It is worth noting that the ZAL layer can be designed either with a real index of $n_p = n_H$ or $n_p = n_L$. In the presented cases, we used n_H, as displayed in the figures. Actually, the condition for the ZAL index is similar to those of the H and L layers, that is, $\sigma < k_p$, which ensures a real effective index required to satisfy (33). Furthermore, the condition $\sigma < k_{H \text{ or } L}$ makes the stationary field to be a combination of trigonometric functions (rather than hyperbolic) within the stack, which allows the specific matrix calculation involving matched quarter-wave layers. It should also be stressed, following (31), that the condition for total reflection on the device only depends on the substrate index n_s, that is, $\sigma > k_s$. This condition ensures that no flux propagates through the substrate, in accordance with the definition of total reflection. Since the field is stationary within the bulk (in the absence of absorption, the real Poynting flux is constant within the bulk for $\sigma < k_s$, and it is zero for $\sigma > k_s$), total reflection at a particular interface within the bulk of the device is not considered.

V. GENERALIZATION TO A MULTILAYER SUBSTRATE: DEPTH LOCALIZATION

By introducing the ZAL concept, we have demonstrated how one may achieve a maximized field bound to the substrate. The ability to create giant enhancement in the near–field region of the substrate allows sensing applications, wherein analyte access to substrate surface is necessary. However, other applications such as microsources require field maximization within the bulk of the stack. Therefore, we now generalize the ZAL principle to field design in the bulk region of dielectric media. We will now demonstrate how replacing the bulk substrate with another multilayer, which we refer to as a

substack (see Fig. 5), will achieve field enhancement within a given layer.

We first note that from (28) that when one admittance is purely imaginary, all admittances are purely imaginary. This result is valid in the absence of absorption, which is the case of our all-dielectric medium. Therefore, all admittances are purely imaginary in the TIR regime ($\sigma > k_s$), since the starting admittance $\tilde{n}_s$ is imaginary (TIR condition). Consequently, the same technique can be used to cancel the admittance of any arbitrary substack illuminated under TIR (Fig. 5). Indeed, formula (33) has just to be modified as

$$\tan \delta_p = \text{Im}(Y_s)/\tilde{n}_p, \qquad (36)$$

where Y_s is the substack admittance, which replaces the former substrate admittance $\tilde{n}_s$.

With this procedure, the shape of the preceding field z distribution is not modified above the substack (see Fig. 6) since the starting admittance ($Y_s = 0$) is not modified for this higher stack. The shape of the field distribution in the lower stack does not depend on the upper stack. The ZAL acts as if the two half stacks (QWS and multilayer substrate) were

FIG. 5. Generalization of the ZAL concept (left) to an arbitrary substack (right).
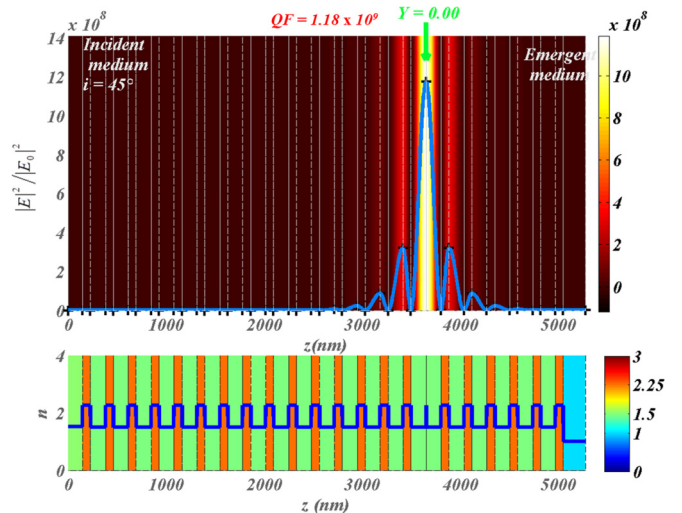
FIG. 6. Theoretical demonstration of huge field enhancement within the bulk of a device implementing the generalized ZAL. The coating is a Q_2 structure deposited on a multilayer QWS substrate, including a ZAL between the two substacks.

turned into quasi-independent structures. Hence more degrees of freedom are available, and this allows one to confine the enhancement within the bulk of the multilayer, as illustrated in Fig. 6 for a Q_2 structure illuminated with TE polarization at 45° incidence. The field is maximum at the ZAL, and the enhancement approaches nine decades. Such control of the enhancement localization within the depth of the coating finds applications in microsource pumping. Notice that the technique can be directly generalized to several ZALs within the stack, hence providing enhancement at different locations. Also, it can be adjusted for arbitrary illumination conditions.

VI. MULTIWAVELENGTH FIELD ENHANCEMENT

Further field design features of relevance to sensing and experiments invoking pump and probe techniques include the ability to achieve multiwavelength or multiangle enhancement. We will therefore explore the ZAL concept further, this time aiming to achieve huge enhancement at several spatial frequencies. We begin by noting that the shape of the field distribution in the lower stack does not depend on the upper stack, a property that we use here at wavelength λ_1. We also note that the ZAL yields an enhancement in the upper stack that is specific but independent of the lower stack, a property that we use at wavelength λ_2. Hence, in the case of several wavelengths, we proceed as follows (see Fig. 7):

(1) A first layer, λ_1 ZAL with refractive index n_p and phase term δ_u, is introduced to cancel the substrate admittance at wavelength λ_1. This ZAL is close to the substrate surface and follows at λ_1:

$$\tan \delta_u = \operatorname{Im}(\tilde{n}_s)/\tilde{n}_p. \tag{37}$$

(2) Then a quarter-wave structure QWS1 is deposited on this λ_1 ZAL, which ensures the enhancement at λ_1, provided that the stack is matched at this wavelength λ_1.

(3) A second layer, λ_2 ZAL with the same refractive index n_p, is deposited on this QWS (see Fig. 7), with a phase term δ_v. This layer is designed to cancel the admittance of the QWS at wavelength λ_2, that is,

$$\tan \delta_v = \operatorname{Im}(Y_s)/\tilde{n}_p. \tag{38}$$
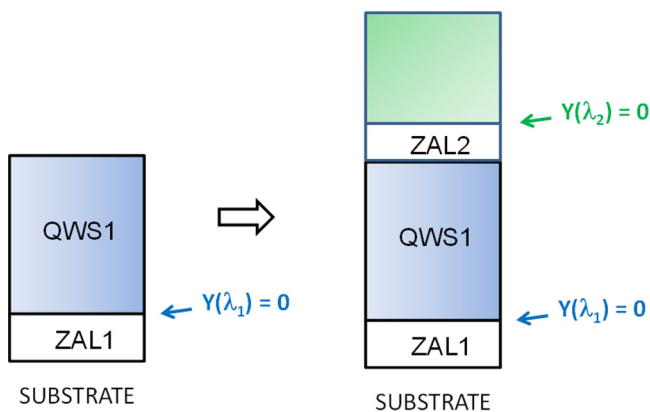
FIG. 7. ZAL for multiwavelength enhancement. Enhancement at wavelength λ_1 (left), and invoking an additional coating, at wavelength λ_2 (right).
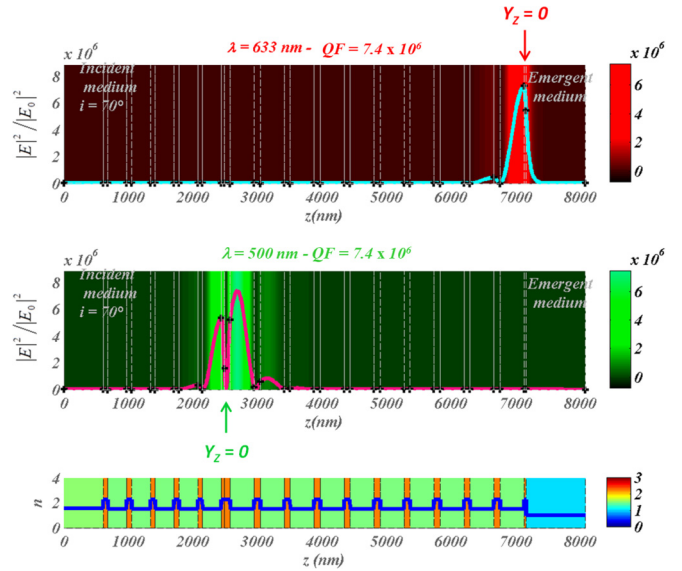
FIG. 8. Introduction of two ZALs provides huge field enhancement at two wavelengths, $\lambda_1 = 633$ nm (top), and $\lambda_2 = 500$ nm (middle).

(4) Finally, above this λ_2 ZAL, a second structure, QWS2, is deposited with layers matched at λ_2 (see Fig. 7).

As confirmed in Fig. 8, the resulting structure provides optimum enhancement at both wavelengths $\lambda_1 = 633$ nm and $\lambda_2 = 500$ nm, for the same illumination angle (70°) and TE polarization. An enhancement value of the order of 10^6 is reached for the two wavelengths. The procedure can be iterated to reach a discrete number of wavelengths. Also, in the same way the procedure works to build stacks, which enhance the field at different angles. Eventually, depth localization can be added to this multiwavelength enhancement.

VII. EXTRINSIC AND INTRINSIC ENHANCEMENT LIMITATIONS

We have shown that the enhancement increases as a $\beta^{\pm N}$ power, with $p = 2N$ or $p = 2N + 1$, the number of layers. Hence there is no upper bound given by the matrix formalism, which raises the question of whether such material media can be realistic. A major limiting factor is intrinsic to the materials, which will not support intense optical fields, due to damage threshold and nonlinear processes [43,44]. Another intrinsic limitation results from absorption processes, which will reduce the enhancement. In Fig. 9, we have plotted the enhancement versus the imaginary index $n'' = n''_H$ of the dielectric films, for different layer numbers of the QWS. As expected, the enhancement value (10^q) is roughly inversely proportional to the imaginary index (10^{-q}) [30]. Since dielectric films with imaginary indices lower than 10^{-5} are feasible [45,46], we first conclude from Fig. 9 that absorption is not a key limitation, as far as realistic enhancements are required.

However, care must be taken with the number of layers, which must be adjusted versus the required enhancement. Let us here denote the enhancement by $|E|^2(n'', p)$. When a
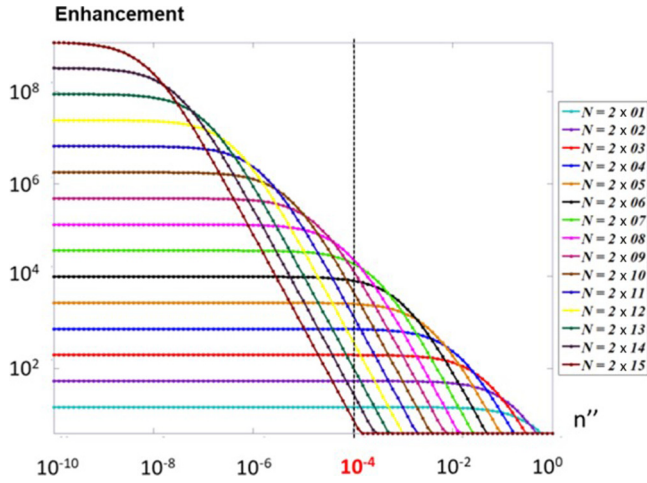
Enhancement

FIG. 9. Enhancement versus the imaginary index, for different layer numbers of the QWS. The H/L materials assumed in the simulations are Ta_2O_5/SiO_2. The incident field is S polarized with a wavelength of 633 nm.

q-decades enhancement is required, a minimum layer number $p_{min}(q)$ is first required; as shown in Fig. 9, for instance, $q = 4$ requires at least $p_{min}(4) = 12$ layers (black curve in Fig. 9)—but for this minimum number there is also a maximum imaginary index $n''_{max}(q)$ at which the enhancement starts to decrease, and which should not be exceeded to maintain the enhancement:

$$n'' < n''_{max}(q) \Leftrightarrow |E|^2[n'', p_{min}(q)] \approx 10^q. \quad (39)$$

In Fig. 9, we have $n''_{max}(q = 4) \approx 10^{-4}$, which means that all imaginary indices lower than 10^{-4} will hold the enhancement to 10^4. However, this is only true for $p_{min}(q) = 12$. This remark stresses the fact that if p is not adjusted and exceeds $p_{min}(q)$ then the imaginary index should be lower than $n''_{max}(q)$ to maintain the enhancement; this can be a major difficulty since it may overpass the performances of the dielectric films having imaginary indices that are hard to produce and to measure below 10^{-6}. To overcome this point, a compromise must be initiated as follows: Since the imaginary index is lower than 10^{-4} for standard coatings, we search for a 10^4 enhancement, which is reached with a minimum of $p = 12$ layers in Fig. 9; once this layer number is fixed, the enhancement will hold for all imaginary indices lower than 10^{-4}, so that the exact knowledge of imaginary indices is not required. In other words, one has to aim at an enhancement given by the lower imaginary index, which can be guaranteed by the thin-film deposition technology.

Beyond these damage and loss phenomena, there is another key limitation, which is extrinsic to materials and originates from the illumination conditions and from the design accuracy. Indeed, huge resonances often cannot be broadband (versus wavelength or angle) so that another compromise must be found with regard to the source characteristics (linewidth $\Delta\lambda_s$ and divergence $\Delta\theta_s$), as well as to the design accuracy (indices and thicknesses). Such compromise means that the coating design should be chosen in such a way that its resonance holds over the whole source band passes. For that, the enhancement now takes an integral
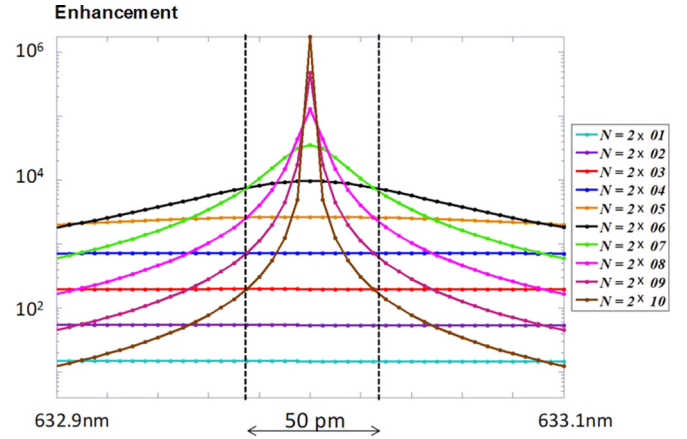
Enhancement

FIG. 10. Enhancement versus wavelength, calculated for different QWS layer numbers. The black curve shows that a 10^4 enhancement can be maintained over a 50-pm-wavelength band pass. The resulting QWS structure involves 12 layers.

form:

$$\left\langle \left| \frac{E(z)}{E_0^+} \right|^2 \right\rangle_{\lambda,\theta} = [1/(\Delta\lambda_s \Delta\theta_s)] \int |E(z,\lambda,\theta)/E_0^+|^2 d\lambda d\theta, \quad (40)$$

with $\Delta\lambda_s$ and $\Delta\theta_s$ the spectral width and the divergence of the source, that is, the illumination band passes of integration. Typically, common laser sources (He-Ne, for instance) often involve characteristics not far from $\Delta\lambda_s \approx 1$ pm and $\Delta\theta_s \approx 1$ mrad. With standard optical filters, such band passes can be neglected since the optical properties of the stack do not vary over them; in other words, for a standard multilayer the source can be assumed to be perfectly monochromatic and parallel. This is no longer true with our specific devices at their huge resonances; indeed, when the enhancement increases with the number p of layers, the bandwidths $(\Delta\lambda_R, \Delta\theta_R)$ of these multilayers decrease in such a way that

$$\lim_{p\to\infty} \Delta\lambda_R = 0, \text{ and } \lim_{p\to\infty} \Delta\theta_R = 0. \quad (41)$$

Therefore, at this level of accuracy, both ratios $\Delta\lambda_R/\Delta\lambda_s$ and $\Delta\theta_R/\Delta\theta_s$ vanish with the number of layers, so that the source must be considered as a broadband source regardless of its band passes. The consequence is that the source characteristics reduce the enhancement when $\Delta\lambda_R/\Delta\lambda_s < 1$ or $\Delta\theta_R/\Delta\theta_s < 1$. The reduced value can be approximated as

$$\left\langle \left| \frac{E(z,p)}{E_0^+} \right|^2 \right\rangle_{\lambda,\theta} \approx \left[\frac{\Delta\lambda_R(p)\Delta\theta_R(p)}{\Delta\lambda_s \Delta\theta_s} \right] |E(z,p,\lambda,\theta)/E_0^+|^2, \quad (42)$$

where p dependence is explicitly included to indicate that while the field increases with p, the band passes decrease with p, emphasizing the compromise to find. As a practical example, we consider here a 10^4 enhancement, as shown in Figs. 10 and 11, where the enhancement is plotted versus illumination wavelength and angle for different QWS layer numbers. The numerical results show that with 12 layers, a 10^4 enhancement can be reached over a spectral band pass of $\Delta\lambda_R = 50$ pm
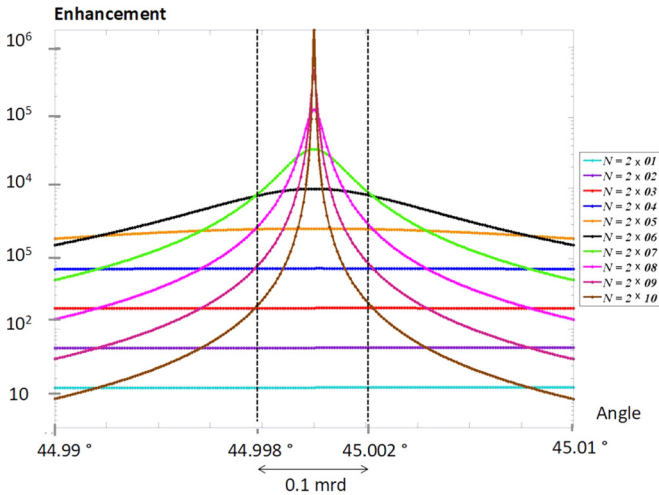
FIG. 11. Enhancement versus illumination angle, calculated for different QWS layer numbers. The black curve shows that a 10^4 enhancement can be maintained over a 0.1-mrad angular band pass. The resulting QWS structure involves 12 layers.

(Fig. 10), which is broader than the band pass of standard lasers. On the other hand, the divergence constraint given in Fig. 11 is more critical ($\Delta\theta_R = 0.1$ mrad) but can be easily obtained at the collimated output of a monomode optical fiber. Therefore, a four-decades enhancement appears to be highly realistic with a QWS of only 12 layers.

Also noteworthy is the design sensitivity. In Fig. 12, we observe that 10^4 enhancement requires a relative accuracy $\Delta e/e \approx 10^{-3}$ on the layer thicknesses. Such accuracy is compatible with the best *in situ* optical monitoring techniques [47,48] that are used today in production of optical thin films. Moreover, this constraint could be released taking into account an error compensation [49], which shifts the optical properties at different angles or wavelengths without altering the field distribution.

However, the uniformity constraints in film production, resulting in thickness variation with position at the coating surface, cannot be ignored. Actually, on the basis of an incident
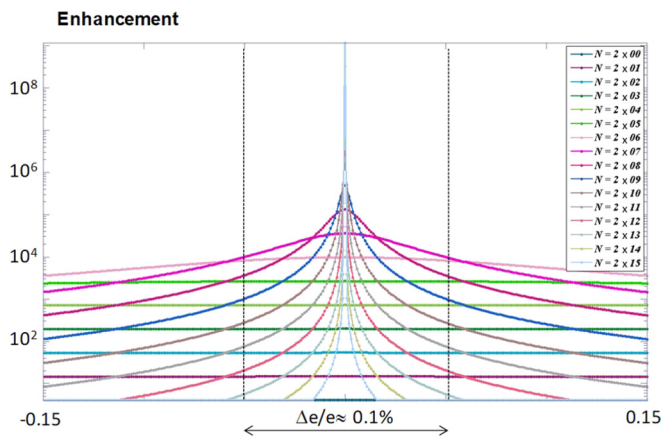
FIG. 12. Enhancement versus thickness accuracy $\Delta e/e$, calculated for different QWS layer numbers. The results show that a 10^4 enhancement can be held over a 0.1% relative error. The resulting QWS structure involves 12 layers.

wave packet, divergence and illuminated area are connected in the form $L \approx \sqrt{2}\,\lambda/(\pi \sin \Delta\theta_s)$ with L the typical dimension of the illumination spot. Since the thickness accuracy must be maintained over the whole illuminated area, this forces the uniformity to be better than 10^{-3} over $L = 6$ mm in the case where $\lambda = 0.6\,\mu$m and $\Delta\theta_s = 0.1$ mrad. This last specification will depend on the geometry of the deposition technology (ion assisted deposition, dual ion beam sputtering, magnetron sputtering, etc.). If necessary, masks can be used to improve the uniformity [50,51]; also, photosensitivity has already been successfully used to correct the uniformity in the case of narrow-band filters [51]. Here, we conclude that design accuracy and uniformity are probably the keys to reach a high enhancement value.

VIII. CONCLUSION

We conclude that the introduced concept of modifying the material response via zero-admittance layers successfully allows the tailoring of giant optical fields within stratified dielectric media under TIR. From the presented analysis, we infer a remarkable flexibility of the ZAL concept with respect to the light polarization. Following the presented results, arbitrarily huge field enhancements can be produced at demand and with depth localization. Also, the concept was shown to be spectrally unlimited allowing enhancements to be produced simultaneously at several wavelengths and for several incidence angles within the same medium. Further configurations are feasible since the substrate can be a multilayer. The analysis of the upper bounds of the enhancement in the considered coatings allowed the evaluation of their performances under realistic conditions. The results clearly indicate that a compromise must be found between the intrinsic limitations (absorption, nonlinearities, and damage threshold) and the extrinsic limitations (spectral and angular illumination band passes, and accuracy of design). A four-decades enhancement was shown to be highly realistic with 12 dielectric layers. The coating uniformity is emphasized to be the key to reach such results. Other phenomena, accompanying the resonances, such as wave-front modification and scattering patterns, which create m lines and bright cones, respectively, warrant further analysis. Clearly, many applications related to optical sensing and microsources can be envisioned. Future work will address the production and characterization of the described material systems. Generalization to microcavities and guided modes will also be considered; indeed, the ZAL layers allow one to engineer resonance frequencies in free space. These frequencies will be quasi-identical to those of the guided modes with large low-index gap. Such property makes the field distribution to be identical for both resonances and guided waves, though normalization is different in the absence of an incident wave.

[1] A. Ranjbar and A. Grbic, Phys. Rev. B **95**, 205114 (2017).

[2] D. Aurelio and M. Liscidini, Phys. Rev. B **96**, 045308 (2017).

[3] C. E. Little, R. Anufriev, I. Iorsh, M. A. Kaliteevski, R. A. Abram, and S. Brand, Phys. Rev. B **86**, 235425 (2012).

[4] A. M. DaSilva, Y.-C. Chang, T. Norris, and A. H. MacDonald, Phys. Rev. B **88**, 195411 (2013).

[5] M. B. Okatan, J. V. Mantese, and S. P. Alpay, Phys. Rev. B **79**, 174113 (2009).

[6] N. J. de Lautour, C. T. Tindle, and S. M. Tan, Phys. Rev. B **70**, 024208 (2004).

[7] A. A. Orlov, A. K. Krylova, S. V. Zhukovsky, V. E. Babicheva, and P. A. Belov, Phys. Rev. A **90**, 013812 (2014).

[8] W. S. Kolthammer, D. Barnard, N. Carlson, A. D. Edens, N. A. Miller, and P. N. Saeta, Phys. Rev. B **72**, 045446 (2005).

[9] J. A. Dionne, L. A. Sweatlock, H. A. Atwater, and A. Polman, Phys. Rev. B **72**, 075405 (2005).

[10] N. Shi and R. Ramprasad, Phys. Rev. B **74**, 045318 (2006).

[11] T. Low, A. S. Rodin, A. Carvalho, Y. Jiang, H. Wang, F. Xia, and A. H. Castro Neto, Phys. Rev. B **90**, 075434 (2014).

[12] L. Sun, Z. Li, T. S. Luk, X. Yang, and J. Gao, Phys. Rev. B **91**, 195147 (2015).

[13] T. Hong, H. Yang, E. K. Gustafson, R. X. Adhikari, and Y. Chen, Phys. Rev. D **87**, 082001 (2013).

[14] Y.-H. Ye, J. Ding, D.-Y. Jeong, I. C. Khoo, and Q. M. Zhang, Phys. Rev. E **69**, 056604 (2004).

[15] V. N. Konopsky, E. V. Alieva, S. Yu. Alyatkin, A. A. Melnikov, S. V. Chekalin, and V. M. Agranovich, Light Sci. Appl. **5**, e16168 (2016).

[16] T. Ling, S.-L. Chen, and L. J. Guo, Opt. Express **19**, 861 (2011).

[17] N. Riesen, T. Reynolds, A. François, M. R. Henderson, and T. M. Monro, Opt. Express **23**, 28896 (2015).

[18] T. Asano, Y. Ochi, Y. Takahashi, K. Kishimoto, and S. Noda, Opt. Express **25**, 1769 (2017).

[19] E. Verhagen, L. Kuipers, and A. Polman, Opt. Express **17**, 14586 (2009).

[20] Z. Yu and S. Fan, Opt. Express **19**, 10029 (2011).

[21] D. Qiu, D. Zhang, Y. Chen, L. Zhu, L. Han, P. Wang, H. Ming, R. Badugu, and J. R. Lakowicz, Opt. Lett. **39**, 4341 (2014).

[22] R. H. Ritchie, Phys. Rev. **106**, 874 (1957).

[23] S. Shukla, S. Prasad, and V. Singh, Phys. Plasmas **22**, 022122 (2015).

[24] *Nanoplasmonic Sensors*, edited by A. Dmitriev (Springer, New York, 2012).

[25] S. A. Maier, *Plasmonics: Fundamentals and Applications* (Springer, New York, 2007).

[26] M. I. Stockman, Opt. Express **19**, 22029 (2011).

[27] H. Iwase, D. Englund, and J. Vučković, Opt. Express **18**, 16546 (2010).

[28] M. Zerrad, A. L. Lereu, C. N'diaye, F. Lemarchand, and C. Amra, Opt. Express **25**, 14883 (2017).

[29] A. L. Lereu, M. Zerrad, C. Ndiaye, F. Lemarchand, and C. Amra, Appl. Opt. **53**, A412 (2014).

[30] C. Ndiaye, F. Lemarchand, M. Zerrad, D. Ausserré, and C. Amra, Appl. Opt. **50**, C382 (2011).

[31] A. L. Lereu, M. Zerrad, A. Passian, and C. Amra, Appl. Phys. Lett. **111**, 011107 (2017).

[32] C. Ndiaye, M. Zerrad, A. L. Lereu, R. Roche, P. Dumas, F. Lemarchand, and C. Amra, Appl. Phys. Lett. **103**, 131102 (2013).

[33] K. Ray, R. Badugu, and J. R. Lakowicz, RSC Adv. **5**, 54403 (2015).

[34] E. Descrovi, A. Angelini, R. Rizzo, F. Frascella, S. Ricciardi, P. Munzert, N. Danz, S. Schmieder, F. Sonntag, M. Alvaro, L. Napione, P. Rivolo, N. de Leo, U. Jonas, F. Michelotti, and F. Bussolino, in *Proceedings of the Conference on Lasers and Electro-Optics: Applications and Technology, San Jose, CA, 2016* (Optical Society of America, Washington, DC, 2016), p. AW4J.5.

[35] F. Michelotti, A. Sinibaldi, N. Danz, F. Frascella, P. Rivolo, P. Mandracci, N. De Leo, F. Giorgis, P. Munzert, U. Schultz, L. Dominici, and E. Descrovi, in *Proceedings of the Latin America Optics and Photonics Conference, Sao Sebtiao, Brazil, 2012* (Optical Society of America, Washington, DC, 2012), p. LS2C.4.

[36] H. A. Macleod, *Thin-Film Optical Filters*, 4th ed. (CRC Press/Taylor & Francis, Boca Raton, FL, 2010).

[37] A. Thelen, *Design of Optical Interference Coatings* (McGraw-Hill, New York, 1989).

[38] Y.-J. Hung and I.-S. Lin, Opt. Express **24**, 16003 (2016).

[39] L. Yu, E. Barakat, T. Sfez, L. Hvozdara, J. Di Francesco, and H. Peter Herzig, Light Sci. Appl. **3**, e124 (2014).

[40] *Optical Interference Coatings*, edited by N. Kaiser and H. K. Pulker (Springer, Berlin, Heidelberg, 2003).

[41] A. V. Tikhonravov, in *Optical Interference Coatings*, edited by N. Kaiser and H. K. Pulker (Springer, Berlin, Heidelberg, 2003), pp. 81–104.

[42] M. Lequime and C. Amra, *De l'Optique électromagnétique à l'interférométrie: Concepts et illustrations* (EDP Sciences, Les Ulis, France, 2013).

[43] J.-Y. Natoli, L. Gallais, H. Akhouayri, and C. Amra, Appl. Opt. **41**, 3156 (2002).

[44] M. Jupé, L. Jensen, A. Melninkaitis, V. Sirutkaitis, and D. Ristau, Opt. Express **17**, 12269 (2009).

[45] M. Commandré and E. Pelletier, Appl. Opt. **29**, 4276 (1990).

[46] B. Li, H. Blaschke, and D. Ristau, Appl. Opt. **45**, 5827 (2006).

[47] M. Lappschies, B. Görtz, and D. Ristau, in *Proceedings of the Conference on Optical Interference Coatings, Tucson, AZ, 2004* (Optical Society of America, Washington, DC, 2004), p. TuE4.

[48] M. Lequime, S. L. Nadji, D. Stojcevski, C. Koc, C. Grézes-Besset, and J. Lumeau, Appl. Opt. **56**, C181 (2017).

[49] B. T. Sullivan and J. A. Dobrowolski, Appl. Opt. **31**, 3821 (1992).

[50] L. Abel-Tibérini, F. Lemarquis, and M. Lequime, Appl. Opt. **47**, 5706 (2008).

[51] W. D. Shen, M. Cathelinaud, M. D. Lequime, F. Charpentier, and V. Nazabal, Opt. Express **16**, 373 (2008).